International Journal of Heat and Mass Transfer 52 (2009) 3353–3363

Contents lists available at ScienceDirect

International Journal of Heat and Mass Transfer

journal homepage: www.elsevier.com/locate/ijhmt

Unsteady fluid mechanics and heat transfer study in a double-tube air–combustor heat exchanger with porous medium

Nelson O. Moraga *, César E. Rosas, Valeri I. Bubnovich, José R. Tobar

Departamento de Ingeniería Mecánica, Universidad de Santiago de Chile, Alameda 3363, Santiago, Chile

ARTICLE INFO

Article history:
Received 29 January 2008
Received in revised form 10 January 2009
Available online 13 March 2009

Keywords:
2D heat transfer
Cylindrical porous combustor
Finite volume simulation

ABSTRACT

Fluid mechanics and heat transfer are studied in a double-tube heat exchanger that uses the combustion gases from natural gas in a porous medium located in a cylindrical tube to warm up air that flows through a cylindrical annular space. The mathematical model is constructed based on the equations of continuity, linear momentum, energy and chemical species. Unsteady fluid mechanics and heat transfer by forced gas convection in the porous media, with combustion in the inner tube, coupled to the forced convection of air in the annular cylindrical space are predicted by use of finite volumes method. Numerical simulations are made for four values of the annular air flow Reynolds number in the range $100 \leqslant Re \leqslant 2000$, keeping constant the excess air $\psi = 4.88$, the porosity $\varepsilon = 0.4$, and the air–fuel mixture inlet speed $Uo = 0.43$ m/s. The results obtained allow the characterization of the velocity and temperature distributions in the inner tube and in the annular space, and at the same time to describe the displacement of the moving combustion zone and the annular porous media heat exchanger thermal efficiency. It is concluded that the temperature increase is directly related to the outer Reynolds number.

1. Introduction

The efficient energy use requires new ways to produce thermal energy from low caloric power fuels, producing low pollutant emissions and with increased heat transfer rates during combustion, with the purpose of reducing energy consumption. The incorporation of porous media favours combustion because this kind of solid material has a thermal conductivity about 100 times greater than that of the gas, in addition to the large heat exchange surface area that exists between solid and fluid. Another advantage of combustion in porous media is the preheating of the gases before arriving at the combustion zone due to radiation and conduction in the solid, resulting in a much more complete combustion since gases arrive at the combustion zone at a much higher temperature than ambient temperature [1–4].

In this field, there are studies that have investigated numerically and experimentally the performance of porous media combustors and the importance of the feedback through the heat recirculation by means of heat transfer from the solid by conduction [5–7] and radiation [8–12]. Other studies have focused on the implementation of a physical mathematical model that allows the development and optimization of the design of burners with porous media [13–20]. Many of these models use a single-step reaction, such as those of Baek [12]; Sathe et al. [13]; Malico and Pereira [14], and Foutko [19], which by means of finite differences method predict the behaviour of the temperature of the solid and the fluid in a porous matrix at 5-min intervals during 25 min using a one-dimensional model. However, there are other models that have used multistep reactions that allow a more accurate prediction of product composition, the energy released, the temperature of the flame, and the temperature profiles. Zhou et al. [21], proposed a 2D combustion model, using a 32-steps chemical reaction that allows for the temperature field prediction.

The use of 2D models for combustion is fundamental due to the complexity of the commercial design of porous media burners, with the purpose of stopping and stabilizing the combustion front. Some of these inert porous media models for burners with integrated cooling tubes are described in the studies of Mohamad et al. [22], Hackert et al. [23] and Barra and Ellzey [24], including a 2D model burner and comparisons with experimental results for two geometries. Another practical example of porous combustor appears in the work of Xuan and Viskanta [25], in which they analyzed numerically a porous matrix burner and succeed in stopping the combustion front by cooling it. In this work, the physical phenomenon is predicted by two energy equations that are along with continuity, two linear momentum equations, the equation of state, and the equation of fuel mass fraction, considering a single-step chemical reaction.

An alternative system for using inert porous media is in heat exchangers with reciprocal flow, developed experimentally by Hoffmann et al. [26] and studied analytically by Sathe et al. [27], Hanamura et al. [28], Park and Kaviany [29], Jughai and Sawananon [30] and Shi et al. [9]. Contarin et al. [31,32] developed a 1D single-step

* Corresponding author. Tel.: +56 2 7183110.
E-mail address: nelson.moraga@usach.cl (N.O. Moraga).

0017-9310/$ - see front matter © 2009 Elsevier Ltd. All rights reserved.
doi:10.1016/j.ijheatmasstransfer.2009.01.010

Nomenclature

Cp	specific heat (J/kg K)
D^M	diffusion coefficient (m^2/s)
dp	pore diameter (m)
Ea	activation energy (J/mol)
h	heat transfer coefficient (W/m^2 K)
h_{RAD}	heat transfer coefficient by radiation (W/m^2 K)
K	frequency factor (1/s)
Le	Lewis number
Nu	Nusselt number
Pr	Prandtl number
p	pressure
Re	Reynolds number
Ro	universal gas constant (J/mol K)
r	radial coordinate
T	temperature (K)
t	time (s)
u_G	gas speed (m/s)
u_{inst}	interstitial gas speed (m/s)
v	velocity (m/s)
w_f	fuel mass fraction
z	axial coordinate

Greek symbols

Δh	combustion enthalpy (J/kg)
α	superficial gas–solid heat exchange coefficient (W/m^3 K)
λ	thermal conductivity (W/m K)
ε	porosity
ε	porous media emissivity
μ	dynamic viscosity of gas (kg/m s)
ρ	density (kg/m^3)
σ	Stephan–Boltzmann constant (W/m^2 K^4)
τ	quartz transmissivity
ψ	excess air

Subscripts

0	initial condition
eff	effective
G	gas
S	solid
in	inconel

mathematical model for this system comparing the model results with the experimental data.

Dobrego et al. [33] studied theoretically, numerically and experimentally the combustion wave inclination instability in a tubular porous media burner. They found that the inclination amplitude growth velocity on the linear stage depended on the combustion wave velocity, the combustor diameter and of the porous media particles diameter.

Moraga et al. [34] studied by using the finite volume method the heat transfer and fluid mechanics in a cylindrical porous media burner, where a combustion process of methane/air mixture takes place, in order to optimize the location of internal heat exchanger devices.

The purpose of this work is to present results of the simulation made with the method of finite volumes to characterize a double-tube air/porous combustor heat exchanger which contains a combustion zone with a porous medium, a heat transfer zone, and an annular zone that receives the heat, where there is a counterflow laminar air flow. The parameters used are $\psi = 4.88$, $\varepsilon = 0.4$, $Uo = 0.43$ m/s in the combustor and $Re = 100$, $Re = 500$, $Re = 1000$, $Re = 2000$ in the annular air flow. The study allows the fluid mechanics and convective heat transport predictions inside the porous media inner combustor and in the annular air flow, determining the temperature increase of the heat exchanger.

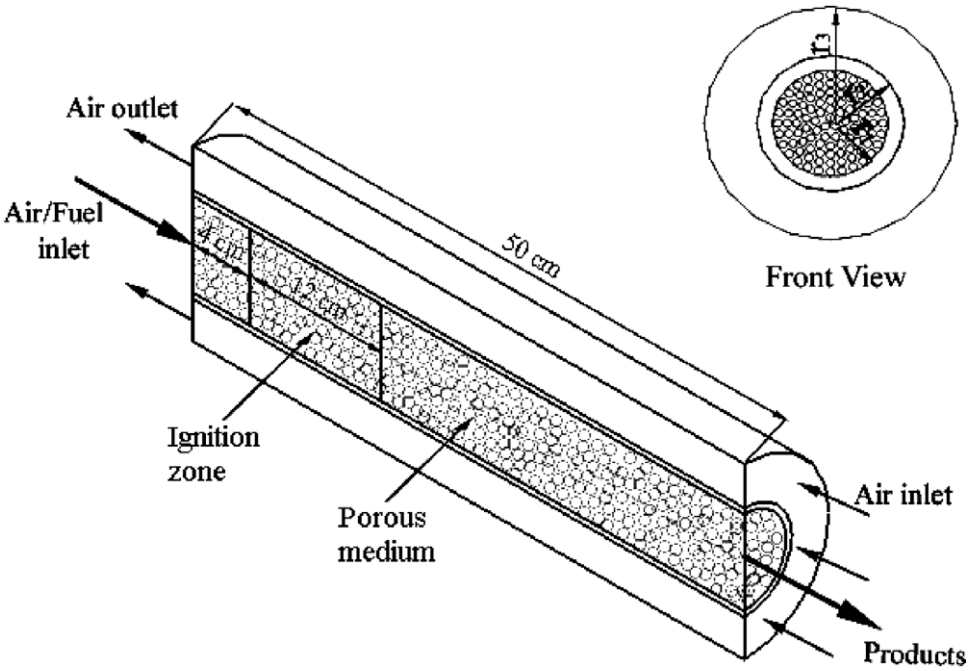

Fig. 1. Double-tube air/porous combustor heat exchanger.

2. Physical layout and mathematical model

Fig. 1 shows the physical layout that describes the cylindrical heat double-tube exchanger. The combustion of methane with air in a porous alumina medium takes place inside the apparatus. The heat generated in the combustion process is used to warm up the counterflow air flow in the cylindrical ring. The mixture of fuel and combustion air enters at room temperature and at a known speed. Inlet temperature air annular flow is 283 K and the inlet velocity varies according to the Reynolds number considered. Combustion takes place in the ignition zone, and CO_2, H_2O, O_2 and N_2 are generated as products. The boundary conditions at the outlet consider that the flow is thermally and hydrodynamically developed. The mixture is considered an ideal gas, and hence that density varies according to the equation of state. In the combustor the following conditions are considered fixed: excess air $\psi = 4.88$, inlet speed $Uo = 0.43$ m/s, and porosity $\varepsilon = 0.4$.

The mathematical model used for the outer flow includes the equations of continuity, linear momentum and energy, for air with constant properties (see Tables 1 and 2).

The mathematical model used for the combustor includes the porosity terms in both the energy equations for the solid as well as for the gas; similarly, also the continuity, linear momentum and fuel mass fraction equations are included. All physical properties are variable with temperature, and it is postulated that density varies according to the ideal gases state equation. The chemical reaction is considered to be in a single-step, with excess air included.

The additional simplifications consider that the fluids are incompressible, the flows are laminar and the fluids are Newtonian. The equations used in the construction of the mathematical model are given below.

2.1. Outer flow equations, for air

Continuity equation

$$\frac{\partial v_r}{\partial r} + \frac{v_r}{r} + \frac{\partial v_z}{\partial z} = 0 \tag{1}$$

Linear momentum in r

$$\rho \cdot \left(\frac{\partial v_r}{\partial t} + v_r \frac{\partial v_r}{\partial r} + v_z \frac{\partial v_r}{\partial z}\right) = -\frac{\partial p}{\partial r} + \mu \cdot \left(\frac{\partial^2 v_r}{\partial r^2} + \frac{1}{r}\frac{\partial v_r}{\partial r} - \frac{v}{r^2} + \frac{\partial^2 v_r}{\partial z^2}\right) \tag{2}$$

Linear momentum in z

$$\rho \cdot \left(\frac{\partial v_z}{\partial t} + v_r \frac{\partial v_z}{\partial r} + v_z \frac{\partial v_z}{\partial z}\right) = -\frac{\partial p}{\partial z} + \mu \cdot \left(\frac{\partial^2 v_z}{\partial r^2} + \frac{1}{r}\frac{\partial v_z}{\partial r} + \frac{\partial^2 v_z}{\partial z^2}\right) \tag{3}$$

Table 1
Properties of inconel and alumina.

Inconel	Alumina
$\lambda_{in} = 0.014 \cdot T + 16.16$ W/m K	$\lambda_s = 1.3$ W/m K

Table 2
Properties of the mixture and of the air.

Mixture	Air
$\rho_G = 1.13$ m^3/kg	$\rho_a = 1.189$ m^3/kg
$Cp_G = 1100$ J/kg K	$Cp_a = 1100$ J/kg K
$\mu_G = 6E-5$ kg/m s	$\mu_a = 1.71E-5$ kg/m s

Energy equation for air

$$\rho \cdot Cp \cdot \left(\frac{\partial T}{\partial t} + v_r \frac{\partial T}{\partial r} + v_z \frac{\partial T}{\partial z}\right) = \lambda \cdot \left(\frac{\partial^2 T}{\partial r^2} + \frac{1}{r}\cdot\frac{\partial T}{\partial r} + \frac{\partial^2 T}{\partial z^2}\right) \tag{4}$$

2.2. Inner porous media combustor equations

Single-step chemical reaction

$$CH_4 + 2(1+\psi)(O_2 + 3.76N_2) \rightarrow CO_2 + 2\cdot H_2O + 2\psi \cdot O_2 + 7.52(1+\psi)N_2 \tag{5}$$

Ideal gas state equation

$$\rho = \frac{\rho_0 \cdot T_0}{T} \tag{6}$$

Continuity equation

$$\frac{\partial(\rho \cdot v_r)}{\partial r} + \frac{\rho \cdot v_r}{r} + \frac{\partial(\rho \cdot v_z)}{\partial z} = 0 \tag{7}$$

Linear momentum in r

$$\frac{\partial(\rho \cdot v_r)}{\partial t} + v_r \frac{\partial(\rho \cdot v_r)}{\partial r} + v_z \frac{\partial(\rho \cdot v_r)}{\partial z} = -\frac{\partial p}{\partial r} + \frac{\partial^2(\mu \cdot v_r)}{\partial r^2} + \frac{1}{r}\frac{\partial(\mu \cdot v_r)}{\partial r} - \frac{\mu \cdot v}{r^2} + \frac{\partial^2(\mu \cdot v_r)}{\partial z^2} \tag{8}$$

Linear momentum in z

$$\frac{\partial(\rho \cdot v_z)}{\partial t} + v_r \frac{\partial(\rho \cdot v_z)}{\partial r} + v_z \frac{\partial(\rho \cdot v_z)}{\partial z} = -\frac{\partial p}{\partial z} + \frac{\partial^2(\mu \cdot v_z)}{\partial r^2} + \frac{1}{r}\frac{\partial(\mu \cdot v_z)}{\partial r} + \frac{\partial^2(\mu \cdot v_z)}{\partial z^2} \tag{9}$$

Table 3
Diffusion coefficient and source terms for the cylindrical 2D model annular flow.

Φ	Γ	Sc	Sp
U	$\frac{\mu}{\rho}$	$\frac{u_{(ant)}}{\Delta t}$	$-\frac{1}{\Delta t}$
V	$\frac{\mu}{\rho}$	$\frac{v_{(ant)}}{\Delta t} - \frac{\mu v}{r^2}$	$-\frac{1}{\Delta t}$
T	$\frac{\mu}{\rho \cdot Pr}$	$\frac{T_{(ant)}}{\Delta t}$	$-\frac{1}{\Delta t}$

Table 4
Diffusion coefficient and source terms for the 2D cylindrical combustor model.

Φ	Γ	Sc	Sp
u	$\frac{\mu_G}{\rho_G}$	$\frac{u_{(ant)}}{\Delta t}$	$-\frac{1}{\Delta t}$
v	$\frac{\mu_G}{\rho_G}$	$\frac{v_{(ant)}}{\Delta t} - \frac{\mu_G v}{r^2}$	$-\frac{1}{\Delta t}$
T_G	$\frac{\mu_G}{(\rho \cdot Pr)_G}$	$\left(\frac{\Delta h \cdot r_f}{(\rho C_p)_G} + \frac{\alpha T_S}{(\rho C_p)_G} + \frac{T_{G(ant)}}{\Delta t}\right)$	$-\left(\frac{\alpha}{(\rho C_p)_G} + \frac{1}{\Delta t}\right)$
w_i	$\frac{\mu_G}{(\rho \cdot Pr)_G}$	$\frac{w_{i(ant)}}{\Delta t}$	$-\left(\frac{K \cdot \exp(-\frac{Ea}{RGT})}{(C_P)_G} + \frac{1}{\Delta t}\right)$
T_S	λ_{eff}	$\left(\alpha T_G + \frac{T_{S(ant)}(\rho Cp)_S}{\Delta t}\right)$	$-\left(\alpha + \frac{(\rho Cp)_S}{\Delta t}\right)$

Table 5
Time steps used in the simulation.

Time (s)	Time steps: Δt (s)
Time < 0.001	$\Delta t = 0.00001$
0.001 < time < 0.01	$\Delta t = 0.0001$
0.01 < time < 0.1	$\Delta t = 0.001$
Time > 0.1	$\Delta t = 0.1$
Time > 20	$\Delta t = 1$

Fuel mass conservation equation

$$\frac{\partial(\rho\cdot w)}{\partial t}+v_r\frac{\partial(\rho\cdot w)}{\partial r}+v_z\frac{\partial(\rho\cdot w)}{\partial z} =\frac{\partial}{\partial r}(D^M\cdot\rho\cdot\frac{\partial w}{\partial r})+\frac{\partial}{\partial z}(D^M\cdot\rho\cdot\frac{\partial w}{\partial z})-\rho\cdot K\cdot w\cdot e^{\frac{-Ea}{Ro\cdot T}} \tag{10}$$

Energy equation for gas in porous medium

$$\varepsilon\cdot\left(\frac{\partial(\rho\cdot Cp\cdot T)}{\partial t}+v_r\frac{\partial(\rho\cdot Cp\cdot T)}{\partial r}+v_z\frac{\partial(\rho\cdot Cp\cdot T)}{\partial z}\right) =-\alpha(T_G-T_S)-\varepsilon\cdot\rho\cdot\Delta h\cdot K\cdot w\cdot e^{\frac{-Ea}{Ro\cdot T}} \tag{11}$$

Energy equation for solid in porous medium

$$(1-\varepsilon)\cdot\left(\frac{\partial(\rho_S\cdot Cp_S\cdot T_S)}{\partial t}\right)=\frac{1}{r}\frac{\partial}{\partial r}\left(r\cdot\lambda_{eff}\frac{\partial T_S}{\partial r}\right) +\frac{\partial}{\partial z}\left(\lambda_{eff}\frac{\partial T_S}{\partial z}\right)+\alpha(T_G-T_S) \tag{12}$$

Reaction speed

$$r_f=w_i\cdot\rho_G\cdot K\cdot\exp\left(-\frac{Ea}{Ro\cdot T}\right) \tag{13}$$

Effective conductivity of the solid

$$\lambda_{eff}=\lambda_S+\lambda_{RAD} \tag{14}$$

Radiation between the solid particles of the porous medium is included by means of the following expression, Foutko et al. [19]

$$\lambda_{RAD}=\frac{32\cdot\sigma\cdot\varepsilon\cdot dp\cdot T^3}{9\cdot(1-\varepsilon)} \tag{15}$$

$$\lambda_{eff}=(1-\varepsilon)\lambda_S+\frac{32\cdot\sigma\cdot\varepsilon\cdot dp\cdot T_S^3}{9\cdot(1-\varepsilon)} \tag{16}$$

The coefficient of convective heat transfer between solid and gas is

$$\alpha=\frac{6(1-\varepsilon)}{dp}\cdot\frac{\lambda_G}{dp}\cdot Nu \tag{17}$$

with

$$\alpha_{Sf}=\frac{6(1-\varepsilon)}{dp} \tag{18}$$

$$u_{Sf}=\frac{\lambda_G}{dp} \tag{19}$$

where the Nusselt number is obtained from the expression

$$Nu=2.0+1.1\cdot(Pr^{1/3}\cdot Re^{0.6}) \tag{20}$$

$$\text{where}\quad Re=\frac{\varepsilon\cdot u\cdot dp\cdot\rho}{\mu} \tag{21}$$

Conjugate boundary conditions between the porous burner section and the annular one are used in the internal and external areas of the inner tube

$$T_i(r_i,z,t)=T_t(r_i,z,t);\quad -\lambda_{eff}\frac{\partial T_i}{\partial r}=-\lambda_t\frac{\partial T_t}{\partial r};$$
$$T_t(r_e,z,t)=T_e(r_e,z,t);\quad -\lambda_t\frac{\partial T_t}{\partial r}=-\lambda_a\frac{\partial T_a}{\partial r} \tag{22}$$

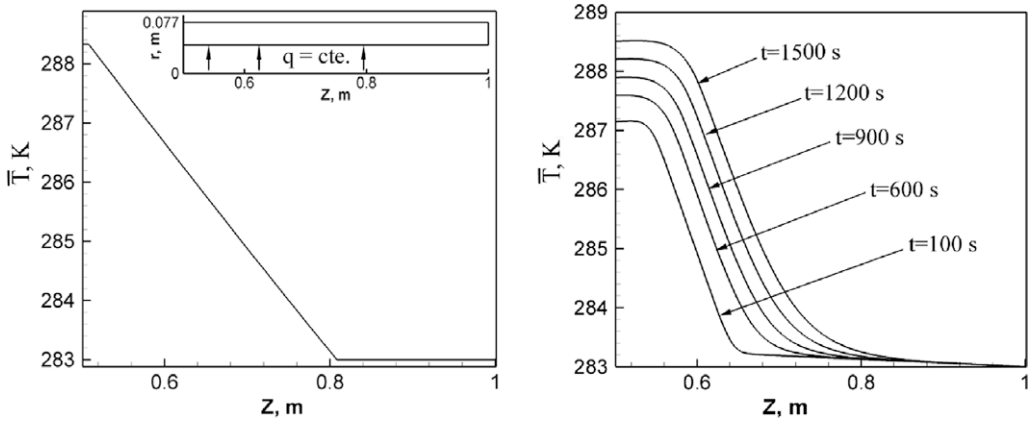

Fig. 2. Air average temperature in the annular flow. On the left, asymptotic case for a constant heat flow along the inner annular wall. On the right, double-tube porous combustor heat exhanger with $\psi = 4.88$, $\varepsilon = 0.4$, $Uo = 0.43$ m/s in the combustor and $Re = 1000$ in the annular flow.

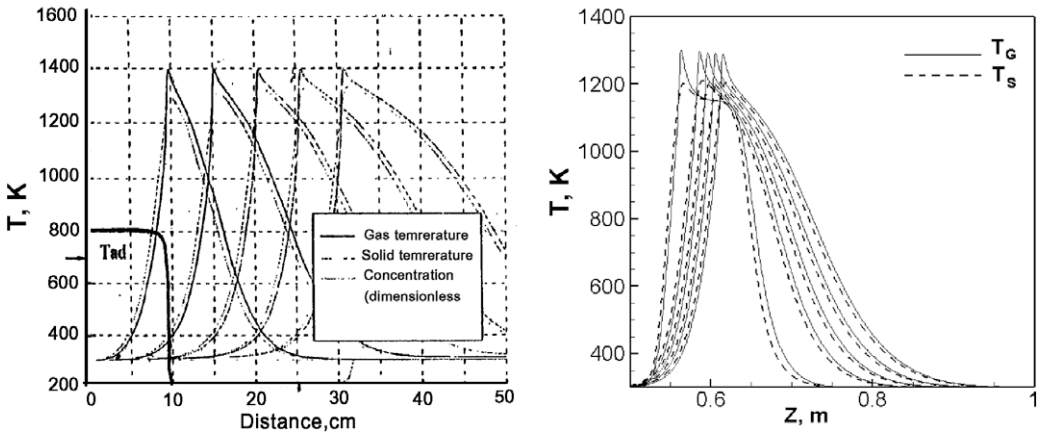

Fig. 3. Evolution of the temperature distribution. On the left, 1D results [19]. On the right, present 2D results in the central axis for $\psi = 4.88$, $\varepsilon = 0.4$, $Uo = 0.43$ m/s.

Additional parameters used in the simulation were the Stephan–Boltzmann constant (σ), combustion enthalpy (Δh_{COMB}), frequency factor (K), activation energy (Ea), and the universal gas constant (Ro), whose respective values are: $\sigma = 5.67 \times 10^8$ W/m^2 K^4; $\Delta h_{COMB} = 50.15 \times 10^6$ J/kg; $K = 2.6 \times 10^8 (1/s)$ and $Ea/Ro = 15643.8$ K.

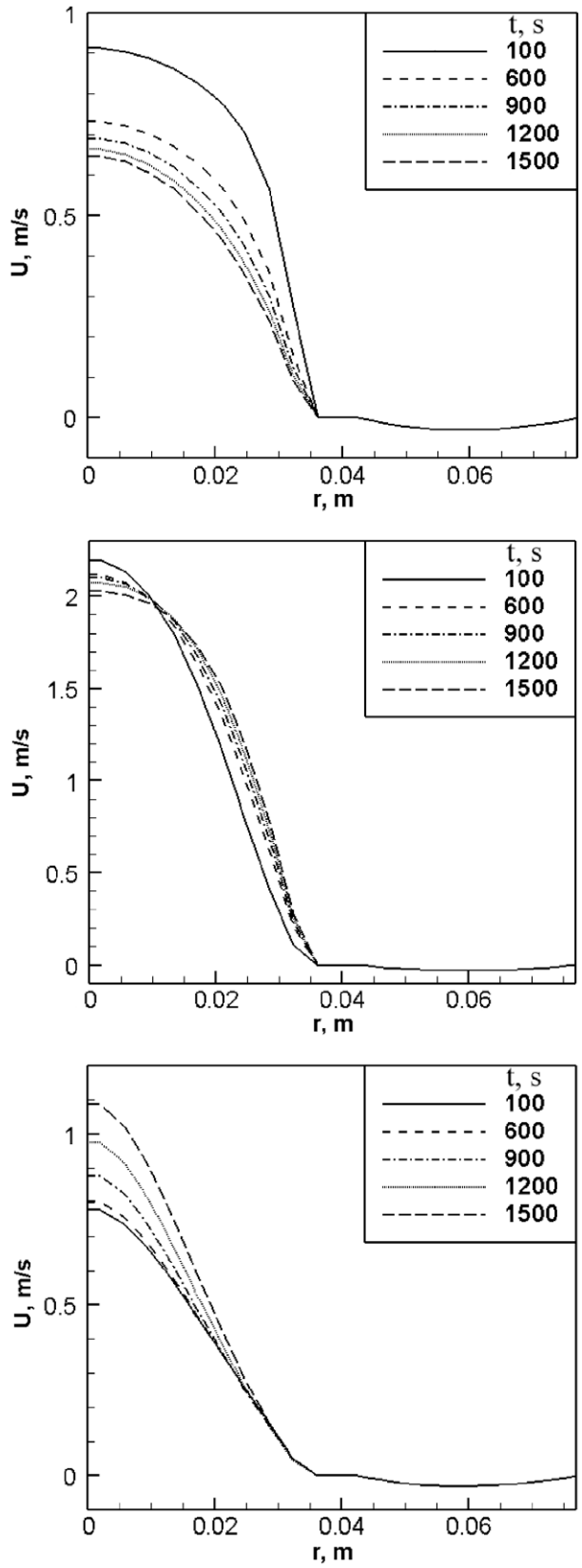

Fig. 4. Axial velocity along the heat exchanger at distances of 0.04 m, 0.14 m and 0.32 m. $\psi = 4.88$, $\varepsilon = 0.4$, $Uo = 0.43$ m/s in combustor, $Re = 100$ in the annulus.

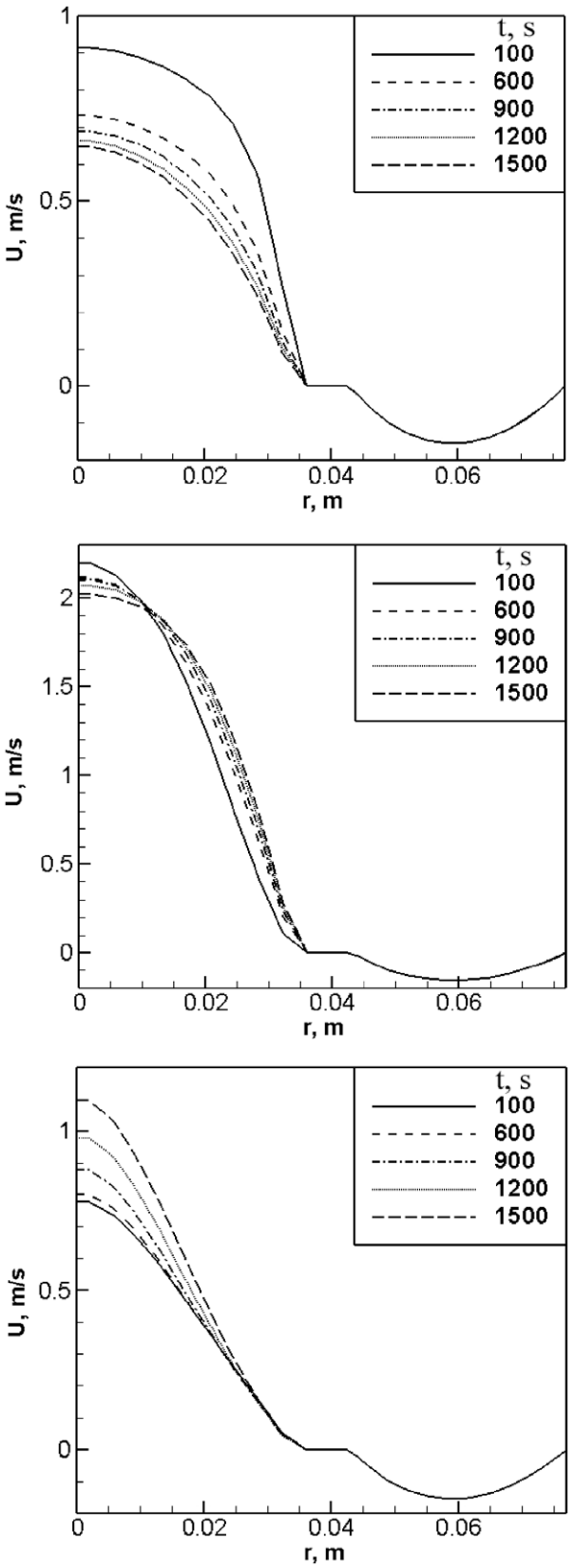

Fig. 5. Axial velocity along the heat exchanger at distances of 0.04 m, 0.14 m and 0.32 m. $\psi = 4.88$, $\varepsilon = 0.4$, $Uo = 0.43$ m/s in combustor, $Re = 500$ in the annulus.

The average temperature in the heat exchanger is calculated by means of

$$\overline{T} = \frac{\int\int u \cdot T \cdot \partial_r \partial_z}{\int\int u \cdot \partial_r \partial_z} \tag{23}$$

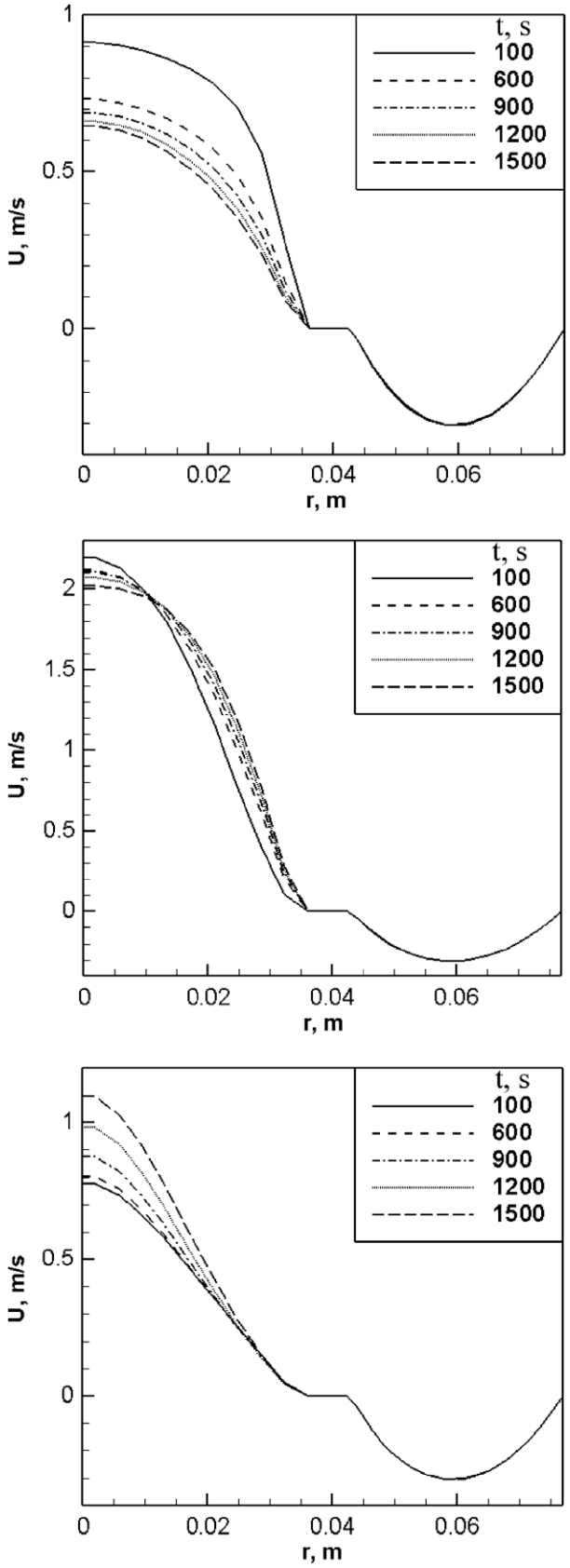

Fig. 6. Axial velocity along the heat exchanger at distances of 0.04 m, 0.14 m and 0.32 m. ψ = 4.88, ε = 0.4, *Uo* = 0.43 m/s in combustor, *Re* = 1000 in the annulus.

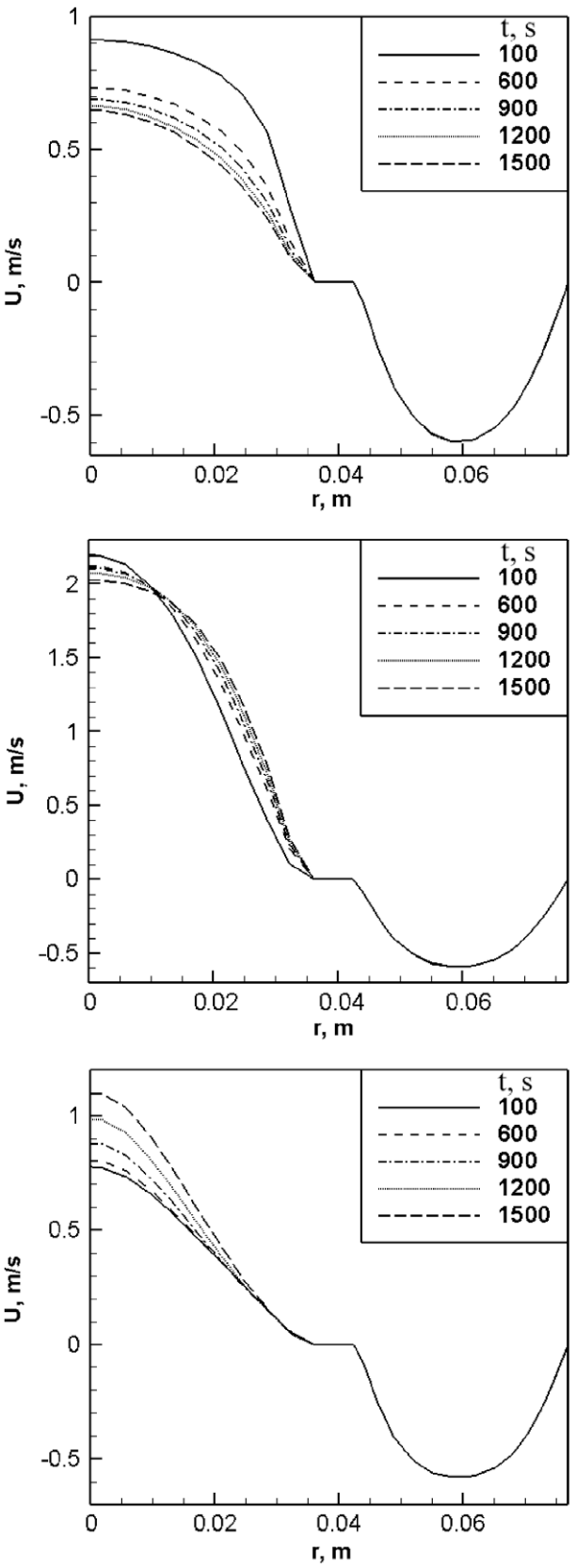

Fig. 7. Axial velocity along the heat exchanger at distances of 0.04 m, 0.14 m and 0.32 m. ψ = 4.88, ε = 0.4, *Uo* = 0.43 m/s in combustor and *Re* = 2000 in the annulus.

The mass diffusion coefficient was found by assuming that the Lewis number was equal to 1,

$$D^M = \frac{\lambda_G}{(\rho \cdot Cp)_G}; \quad (Le = 1); \quad \lambda_G = \frac{\mu \cdot Cp}{Pr}; \quad D^M = \frac{\mu}{\rho \cdot Pr} \tag{24}$$

Inlet and outlet boundary conditions of the heat exchanger are:

$$Z = 0.0, \quad \text{when} \begin{cases} 0 \leqslant r \leqslant 0.038 & \Rightarrow U_0 = 0.43 \wedge T = 300K \\ 0.038 \leqslant r \leqslant 0.077 & \Rightarrow \frac{\partial u}{\partial z} = \frac{\partial T}{\partial z} = 0 \end{cases}$$
$$Z = 1.5, \quad \text{when} \begin{cases} 0 \leqslant r \leqslant 0.038 & \Rightarrow U_0 = 0.43 \wedge T = 300K \\ 0.038 \leqslant r \leqslant 0.077 & \Rightarrow U_0 = \frac{Re \cdot v}{D_h} \wedge T = 283K \end{cases} \tag{25}$$

3. Solution procedure

The system of equations that governs this problem is solved numerically using the finite volume method by means of the SIMPLE algorithm, Patankar [35].

Each one of the governing equations was written in the general form of the transport equation, with unsteady, convective, diffusion and linearized source terms:

$$\frac{\partial(\rho \cdot \phi)}{\partial t} + div(\rho \cdot \vec{v} \cdot \phi) = div(\Gamma \cdot grad\phi) + Sc + Sp \cdot \phi \tag{26}$$

The diffusion coefficient (Γ) and the source terms (Sc, Sp) for each dependent variable Φ are given in Tables 3 and 4.

The convergence criteria used for gas and solid temperature and for fuel mass fraction are

$$|\phi_{i,j}^k - \phi_{i,j}^{k-1}| \leqslant 10^{-3} \tag{27}$$

while for the two velocity components a more restrictive criterion was imposed

$$|\phi_{i,j}^k - \phi_{i,j}^{k-1}| \leqslant 10^{-4} \tag{28}$$

where Φ is the dependent variable and k is the level of iteration at a given time. The staggered non uniform grid used has 652×26 nodes in the axial and radial directions, respectively. The subrelaxation coefficients used were equal to 0.1 for the u and v velocity components, and 0.5 for the gas and solid temperature and for the fuel fraction.

Calculations were accomplished in a 2.4 GHz Intel Xeon® personal computer with 2.0 GB of RAM.

A strategy based on the use of dynamic time steps was implemented. The different values of the time steps used in the unsteady calculations are given in Table 5.

4. Results and discussion

The numerical simulation main objective was the prediction of the unsteady velocity and temperature profiles in the heat exchanger.

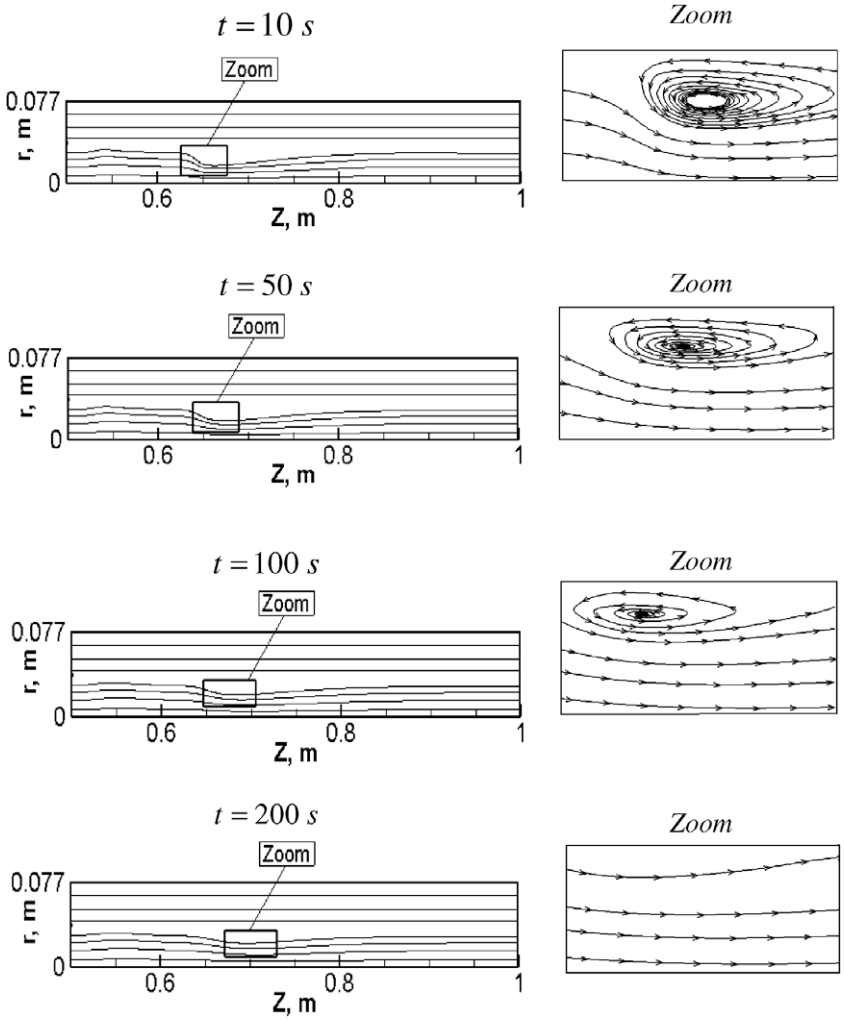

Fig. 8. Streamlines at different times for $\psi = 4.88$, $\varepsilon = 0.4$, $Uo = 0.43$ m/s in the combustor and $Re = 2000$ in the annular flow.

The effect of the outer Reynolds number on the temperature increase of the air in the annular flow was also investigated. Porous media combustion investigated originated a combustion wave that moved towards the tube exit, in a super-adiabatic regime [28]. Air moving in a counterflow inside the annular cylindrical domain (external concentric tube) contributed to stop the wave propagation due to heat removal. The unsteady state influences the heat transfer characteristics in the double-tube heat exchanger proposed in four main ways: (a) fuel–air mixture pre-heating at the tube inlet caused by heat propagation to the inlet by conduction through the solid particles (allumina spheres) of the porous media [36]; (b) pollutants reduction in the high temperature porous media, due to post-combustion of the gases, by radiation, conduction and forced convection, in the space between the moving ignition region and the tube exit [30]; (c) air heating rate in the external tube; and (d) to understand the main characteristics of this type of combustors: flame stability (shape, inclination and structure), combustion wave displacement velocity and initial and final accelerations [32,37–41].

Figs. 2 and 3 show results for asymptotic cases of the heat exchanger. Fig. 2 shows air flow in the annular flow when the pipe is heated from the bottom. Predicted results are compared with the results obtained in the heat exchanger at a time of 1500 s, showing a 0.06% deviation for the average temperature of the outer flow at the heat exchanger outlet. In Fig. 3, predicted unsteady temperature profiles in the combustor calculated in this work using the 2D model, are compared to the results obtained by the 1D model used by Foutko [19]. The average deviation of the maximum temperature along the central axis of the combustor with respect to that calculated by Foutko [19] is 7% for the gas temperature and of 7.7% for the solid temperature. Present calculations shows that combustion front is located at an axial position of 0.115 m from the inlet, at time t = 1500 s, while a position of 0.3 m was predicted by Foutko [19] with the 1D model.

Fig. 4 shows that the axial component of the velocity at the beginning of the combustion zone, located at a distance of 0.04 m from the inlet of the heat exchanger, has values near 1 m/

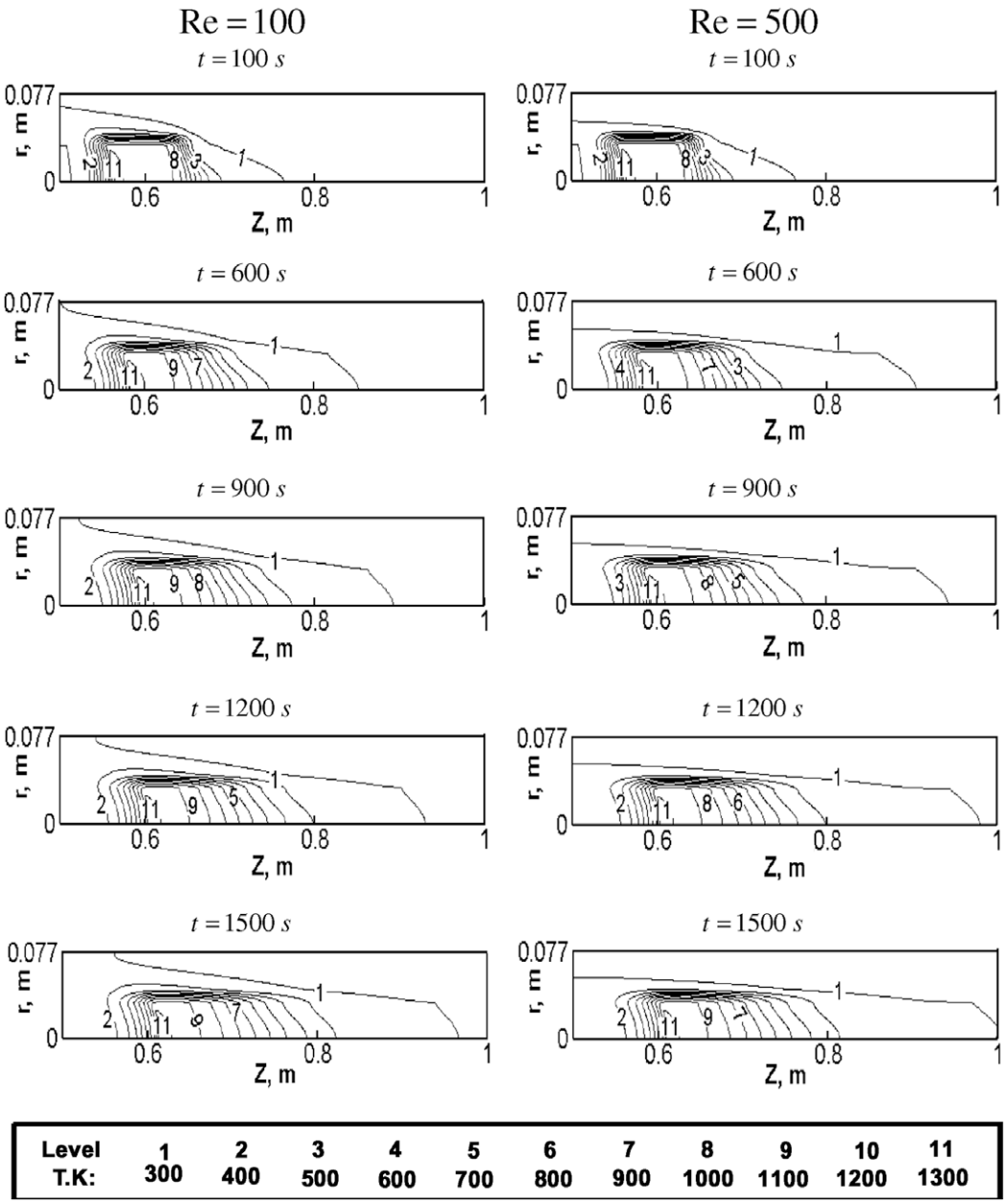

Fig. 9. Effect of the outer Reynolds number on the heat exchanger temperature field, with ψ = 4.88, ε = 0.4, Uo = 0.43 m/s in the combustor, Re = 100 and 500.

s in a time of 100 s. As time goes by, the speed decreases because the combustion zone is displaced toward the combustor outlet, reaching a value of 0.65 m/s at a time of 1500 s. In the axial position, at 0.14 m of the inlet, the velocity remains close to 2 m/s, inside the combustion zone, where temperature is highest. But at a distance of 0.32 m from the inlet the axial velocity starts increasing with time due to the combustion front displacement. On the other hand, the velocity in the annular flow remains constant throughout the whole heat exchanger with a value near to 0.03 m/s. Figs. 5–7 show similar trends when the annular Reynolds number increase from 500 to 2000 with higher velocities of 0.15 m/s, 0.31 m/s and 0.59 m/s, respectively.

Fig. 8 shows the flow lines of the heat exchanger at times of $t = 100$ s, $t = 200$ s, $t = 400$ s and $t = 800$ s. The zone where the secondary flows appear, causing the recirculation of flows in the combustor at a distance of 0.175 m from the combustor inlet is seen. The secondary flows are attenuated as time goes by and at time $t = 800$ s they have already disappeared.

Figs. 9 and 10 show the effect of the Reynolds number on the temperature fields in the heat exchanger. The displacement of the combustion front is shown at times $t = 100$ s, $t = 600$ s, $t = 900$ s, $t = 1200$ s and $t = 1500$ s. The results show that the combustion front displacement is independent of the Reynolds number. Isotherm 1 ($T = 300$ K) in the annular air flow changes with time when $Re = 100$, and the displacement of the isotherm $T = 300$ K becomes almost imperceptible at $Re = 2000$. Fig. 11 illustrates the variation with time of the annular air mean temperature for Reynolds numbers of $Re = 100$, $Re = 500$, $Re = 1000$ and $Re = 2000$. In all cases the mean temperature increases as time goes by.

Air heating in the annular space of the exchanger is shown in Table 6. There is a dramatic decrease in the air heating when the

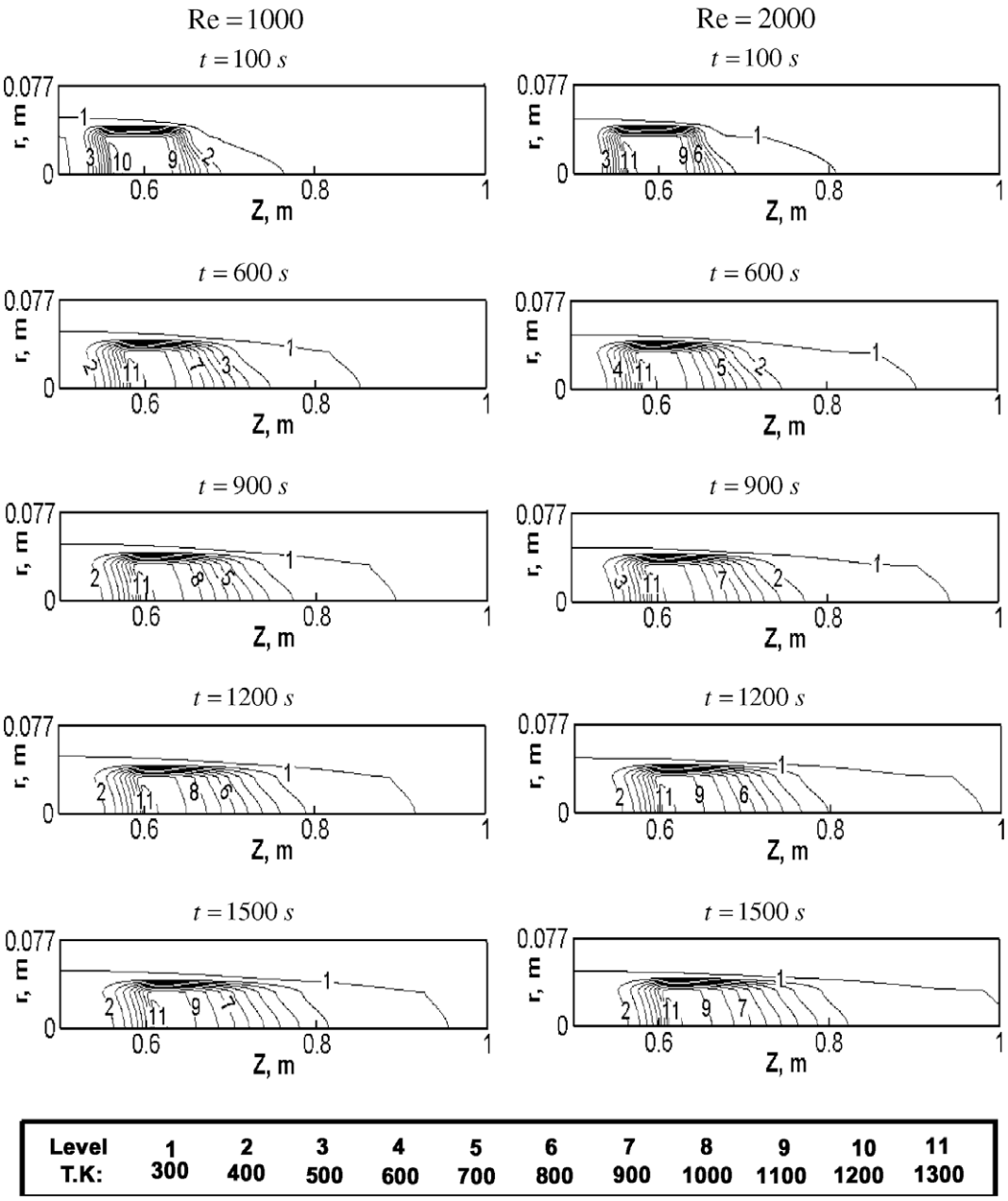

Fig. 10. Effect of the outer Reynolds number on the heat exchanger temperature field, with $\psi = 4.88$, $\varepsilon = 0.4$, $Uo = 0.43$ m/s in the combustor, Re = 1000 and 2000.

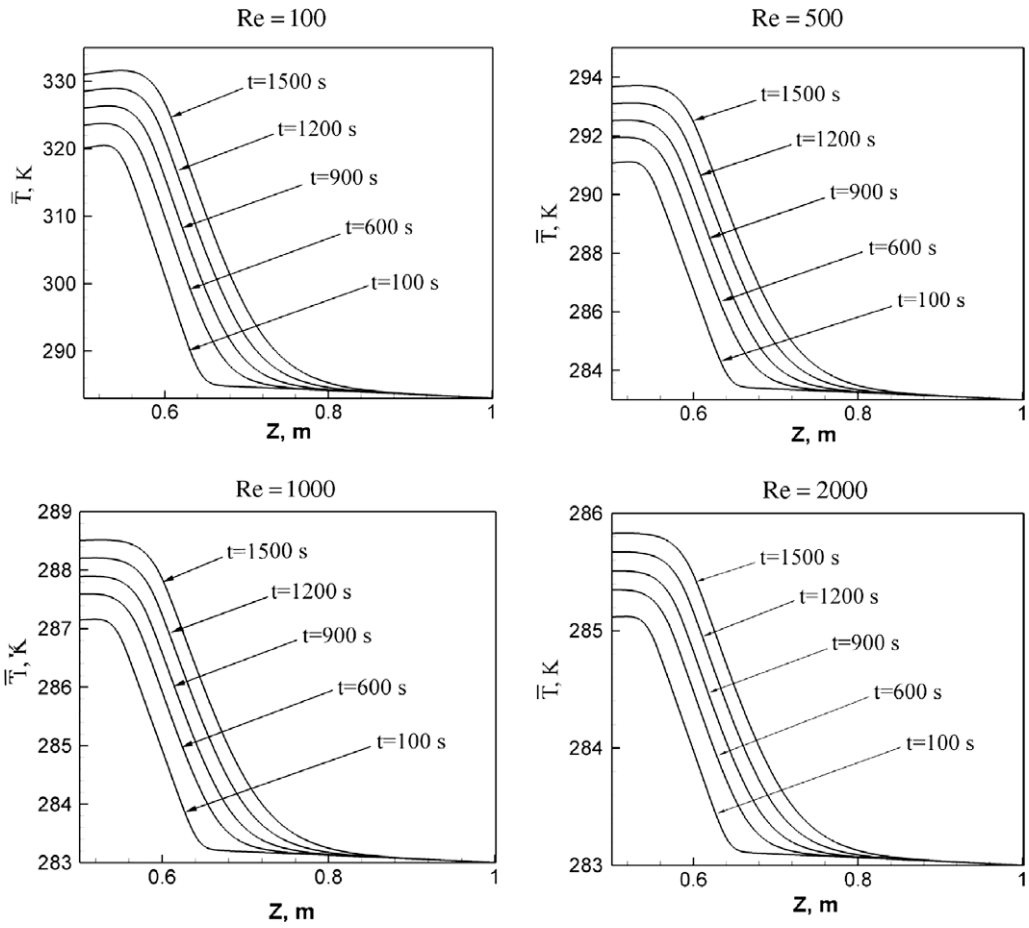

Fig. 11. Effect of the outer Reynolds number on the outer flow average temperature, with $\psi = 4.88$, $\varepsilon = 0.4$, $Uo = 0.43$ m/s in the combustor.

Table 6
Temperature difference of the external fluid between the inlet and outlet.

Time (s)	ΔT (K)			
	$Re = 100$	$Re = 500$	$Re = 1000$	$Re = 2000$
100	37.1	8.1	4.1	2.1
600	40.5	8.9	4.6	2.3
900	43	9.5	4.9	2.5
1200	45.5	10.1	5.2	2.7
1500	48	10.7	5.5	2.8

outer Reynolds number increases. Significant temperature differences were found between the maximum ($Re = 2000$) and minimum ($Re = 100$) outer Reynolds numbers, which increased the average outer temperature of the air flow by 37 K when $Re = 100$ and 2 K when $Re = 2000$, at a time of 100 s, keeping this proportion at later times.

Heat performance was studied in terms of the heat exchanger effectiveness, defined as the ratio between air heating rate and the thermal energy provided by methane combustion, 8.03×10^5 kJ/kmol [42]. The double-tube heat exchanger effectiveness η, calculated for the base case defined in Fig. 1, with $Uo = 0.43$ m/s, $Re = 2000$, $\varepsilon = 0.4$, $\Psi = 4.88$, was 13.8%. In addition, the effectiveness for three alternative designs was determined: air internal re-circulation in an inner tube (diameter equal to 0.0152 m), with $\eta = 28.1\%$; simultaneous external and internal air flows, with $\eta = 19.3\%$ and inner air flow with porous media in the annular external region, with $\eta = 36.7\%$. Effectiveness experimental values reported by Xuan and Viskanta [25], for a porous matrix methane combustor with embedded coolant tubes, were found to decrease from 70% to 30% when the firing rate increased from 10 to 60 kW. Finite volume calculations, with the SIMPLER algorithm and a mathematical model developed by Mohamad et al. [22], for the same combustor–heater system with coolant tubes, shows that thermal efficiency can change from 55% to 22%, due to variations in the particle diameter ratio. Thermal efficiencies in the range of 45–80% have been reported by Contarin et al. [31] for a reciprocal flow filtration methane combustor with embedded heat exchangers, depending on the equivalence ratio and filtration velocity. The heat recirculation efficiency, defined as the ratio between solid-to-gas convection in preheat zone and the firing rate, has been examined by Barra and Ellzey [24], for a porous methane burner with partially stabilized zirconia, with efficiencies between 6 and 25%, depending on the flame speed and the equivalence ratio. Thermal efficiency for a cyclic flow reversal porous media combustor has been found to be almost twice higher than conventional one-way flow combustors, Jugjai and Sawananon [30]. Even though the thermal efficiency calculated for the proposed double-tube air-porous medium combustor heat exchangers was in the range between 14% and 37%, further improvements can be expected by using fins.

5. Conclusions

Numerical simulations were made for four values of the annular flow Reynolds number, for $Re = 100$, 500, 1000 and 2000, keeping constant the excess air $\psi = 4.88$, porosity $\varepsilon = 0.4$ and inlet speed $Uo = 0.43$ m/s in the porous media combustor. The results obtained with the 2D model presented here, differs greatly from those ob-

tained with the 1D previous model. Temperature differences calculated with the present 2D model are 7% larger for both the gas and the solid, than those results obtained with 1D models. The instantaneous position calculated with the 1D models shows that the combustion front moves 2.6 times faster than in the 2D model.

The axial velocity of the combustor is not affected by the Reynolds number of the air flow in the external annular space. However in this annular region the axial velocity of the air flow increases 20 times when the Reynolds number increases from $Re = 100$ to $Re = 2000$.

The 2D model presented here allows the secondary flows to be captured in the porous media combustor. The secondary flows appear at the beginning of the combustion because of the formation of the combustion front, but as time goes by they tend to disappear.

In the annular air flow the average temperature increment is directly related to the decrease of the calculated Reynolds numbers. As the Reynolds number increases from $Re = 100$ to $Re = 2000$, the mean temperature increases at the outlet of the heat exchanger by 40 K on the average for the calculated times.

Acknowledgements

The authors acknowledge to CONICYT–Chile for support received in the FONDECYT 1040148 and 1070186 projects.

References

[1] P. Dubertaki, H.W. Hsu, Stagnation point heat transfer: ignition of a combustible mixture with inert gas injection through a porous wall, J. Heat Transfer 97 (1975) 626–627.
[2] O.S. Rabinovich, I.G. Gurevich, Low-temperature technology combustion of porous systems with forced filtration of a gas reagent, Int. J. Heat Mass Transfer 29 (1986) 241–255.
[3] V.V. Martynenko, R. Echigo, H. Yoshida, Mathematical model of self-sustaining combustion in inert porous medium with phase change under complex heat transfer, Int. J. Heat Mass Transfer 41 (1998) 117–126.
[4] S.A. Zhdanok, K.V. Dobrego, S.I. Futko, Effect of porous media transparency on spherical and cylindrical filtrational combustion heaters performance, Int. J. Heat Mass Transfer 43 (2000) 3469–3480.
[5] M. Katsuki, T. Hasegawa, The science and technology of combustion in highly preheated air, in: 27th Symposium International on Combustion, Belorus, 1998, pp. 3135–3146.
[6] C.Y.H. Chao, J.H. Wang, W. Kong, Effects of fuel properties on the combustion behaviour of different types of porous beds soaked with combustible liquid, Int. J. Heat Mass Transfer 47 (2004) 5201–5210.
[7] T.K. Kayal, M. Chakrabarty, Combustion of liquid fuel inside inert porous media: an analytical approach, Int. J. Heat Mass Transfer 48 (2005) 331–339.
[8] T.K. Kayal, M. Chakrabarty, Modeling of trickle flow liquid fuel combustion in inert porous medium, Int. J. Heat Mass Transfer 49 (2006) 975–983.
[9] J.R. Shi, M.Z. Xie, G. Li, H. Liu, J.T. Liu, H.T. Li, Approximate solutions of lean premixed combustion in porous media with reciprocating flow, Int. J. Heat Mass Transfer 52 (2009) 702–708.
[10] T.K. Kayal, M. Chakrabarty, Combustion of suspended fine solid fuel in air inside inert porous medium: a heat transfer analysis, Int. J. Heat Mass Transfer 50 (2007) 3359–3365.
[11] T.K. Kayal, M. Chakrabarty, Modeling of a conceptual self-sustained liquid fuel vaporization–combustion system with radiative output using inert porous media, Int. J. Heat Mass Transfer 50 (2007) 1715–1722.
[12] S. Baek, The premixed flame in a radiatively active porous medium, Combust. Sci. Tech. 64 (1989) 277–281.
[13] S. Sathe, R. Peck, T. Tong, Flame stabilization and multimode heat transfer in inert porous media, Combust. Sci. Tech. 70 (1990) 93–109.
[14] I. Malico, J.C.F. Pereira, Numerical study on the influence of radiative properties in porous media combustion, J. Heat Transfer 123 (2001) 951–957.
[15] P. Hsu, W. Evans, J. Howell, Experimental and numerical study of premixed combustion within nonhomogeneous porous ceramics, Combust. Sci. Tech. 90 (1993) 149–172.
[16] P. Bouma, R. Eggels, L. Goey, J. Nieuwenhuizen, A. Van Der Drift, A numerical and experimental study of the NO-emission of ceramic foam surface burners, Combust. Sci. Tech. 108 (1995) 193–203.
[17] X. Zhou, J. Pereira, Numerical study of combustion and pollutants formation in inert nonhomogeneous porous media, Combust. Sci Tech. 130 (1997) 335–364.
[18] I. Malico, X. Zhou, J. Pereira, Two-dimensional numerical study of combustion and pollutants formation in porous burners, Combust. Sci. Tech. 152 (2000) 57–79.
[19] S. Foutko, S. Shabunya, S. Zhdanok, Superadiabatic combustion in a diluted methane air mixture under filtration in a packed bed, in: 26th Symposium International on Combustion, Belorus, 1996.
[20] P. Hsu, R. Matthews, The necessity of using detailed kinetics in models for premixed combustion within porous media, Combust. Flame 93 (1993) 157–166.
[21] X. Zhou, G. Brenner, T. Weber, F. Durst, Finite-rate chemistry in modelling of two-dimensional jet premixed CH_4/air flame, Int. J. Heat Mass Transfer 42 (1999) 1757–1773.
[22] A.A. Mohamad, S. Ramadhyani, R. Viskanta, Modelling of combustion and heat transfer in packed bed with embedded coolant tubes, Int. J. Heat Mass Transfer 38 (1994) 1181–1191.
[23] C.L. Hackert, J.L. Ellzey, O.A. Ezekoye, Combustion and heat transfer model in two dimensional porous burners, Combust. Flame 116 (1999) 177–191.
[24] A.J. Barra, J.L. Ellzey, Heat recirculation and heat transfer in porous burners, Combust. Flame 137 (2004) 230–241.
[25] Y. Xuan, R. Viskanta, Numerical investigation of a porous matrix combustor–heater, Numer. Heat Transfer A 36 (1999) 359–371.
[26] J. Hoffman, R. Echigo, H. Yoshida, S. Tada, Experimental study on combustion in porous media with a reciprocating flow system, Combust. Flame 111 (1997) 32–46.
[27] S.B. Sathe, R.E. Peck, T.W. Tong, A numerical analysis of heat transfer and combustion in porous radiant burners, Int. J. Heat Mass Transfer 33 (1990) 1331–1338.
[28] K. Hanamura, R. Echigo, S.A. Zhdanok, Superadiabatic combustion in a porous medium, Int. J. Heat Mass Transfer 36 (1993) 3201–3209.
[29] C.W. Park, M. Kaviany, Evaporation–combustion affected by in-cylinder, reciprocating porous regenerator, J. Heat Transfer 124 (2002) 184–194.
[30] S. Jugjai, A. Sawananon, The surface combustor–heater with cyclic flow reversal combustion embedded with water tube bank, Fuel 83 (2004) 2369–2379.
[31] F. Contarin, W. Barcellos, A. Saveliev, L. Kennedy, Energy from a porous media reciprocal flow burner with embedded heat exchangers, J. Heat Transfer 127 (2005) 123–130.
[32] F. Contarin, A.V. Savaliev, A.A. Fridman, L.A. Kennedy, A reciprocal flow filtration combustor with embedded heat exchangers: numerical study, Int. J. Heat Mass Transfer 46 (2003) 949–961.
[33] K. Dobrego, I. Koslov, V. Bubnovich, C. Rosas, Dynamics of filtration combustion front perturbation in the tubular porous media burner, Int. J. Heat Mass Transfer 46 (2003) 3279–3289.
[34] N.O. Moraga, C.E. Rosas, V. Bubnovich, N. Solari, On predicting two-dimensional heat transfer in a cylindrical porous media combustor, Int. J. Heat Mass Transfer 51 (2008) 302–311.
[35] S. Patankar, Numerical Heat Transfer and Fluid Flow, Hemisphere, Washington, 1980.
[36] Y. Huang, C.Y.H. Chao, P. Cheng, Effects of preheating and operation conditions on combustion in a porous medium, Int. J. Heat Mass Transfer 45 (2002) 4315–4324.
[37] M. Sahroui, M. Kaviany, Direct simulation vs volume-averaged treatment of adiabatic, premixed flame in a porous medium, Int. J. Heat Mass Transfer 37 (1994) 1834–2817.
[38] G. Brenner, K. Pickenäcker, O. Pickenäcker, D. Trimis, K. Wawrzinek, T. Weber, Numerical and experimental investigation of matrix-stabilized methane/air combustion in porous inert media, Combust. Flame 123 (2000) 201–213.
[39] A.J. Barra, G. Diepvens, J.L. Ellzey, M.R. Henneke, Numerical study of the effects of material properties on flame stabilization in a porous burner, Combust. Flame 134 (2003) 369–379.
[40] J.F. Liu, W.H. Hsieh, Experimental investigation of combustion in porous heating burners, Combust. Flame 138 (2004) 295–303.
[41] N.A. Kakutkina, Some stability aspects of gas combustion in porous media, Combust. Explosion Shock Waves 41 (2005) 395–404.
[42] R.O. Buckius, Fundamentals of Engineering Thermodynamics, McGraw-Hill, New York, 1992. p. 127.